

RSC Advances



This is an *Accepted Manuscript*, which has been through the Royal Society of Chemistry peer review process and has been accepted for publication.

Accepted Manuscripts are published online shortly after acceptance, before technical editing, formatting and proof reading. Using this free service, authors can make their results available to the community, in citable form, before we publish the edited article. This *Accepted Manuscript* will be replaced by the edited, formatted and paginated article as soon as this is available.

You can find more information about *Accepted Manuscripts* in the [Information for Authors](#).

Please note that technical editing may introduce minor changes to the text and/or graphics, which may alter content. The journal's standard [Terms & Conditions](#) and the [Ethical guidelines](#) still apply. In no event shall the Royal Society of Chemistry be held responsible for any errors or omissions in this *Accepted Manuscript* or any consequences arising from the use of any information it contains.

Influence of Al₂O₃ Nanoparticles Embedded-TiO₂ Nanofibers based Photoanodes on Photovoltaic Performance of a Dye Sensitized Solar Cell

Zaahir Salam, E.Vijayakumar, A.Subramania*

*Electrochemical Energy Research Lab, Centre for Nanoscience and Technology,
Pondicherry University, Puducherry - 605 014, India.*

(*Corresponding Author E-mail: a.subramania@gmail.com)

Tel: +91-413-2654980, Fax(+91)413-2655348

ABSTRACT

Different weight percentages (1, 3 and 5wt %) of Al₂O₃ nanoparticles (NPs) embedded TiO₂ nanofibers (NFs) were prepared by the electrospinning technique. A mixture of titanium isopropoxide, acetic acid, Al₂O₃ NPs and PVP in ethanol were used. X-ray diffraction studies confirmed the formation of anatase and mixed phase (anatase/rutile) for pure TiO₂ NFs and Al₂O₃ NPs embedded TiO₂ NFs, respectively. SEM and TEM studies showed that the morphologies of Al₂O₃ NPs embedded TiO₂ NFs and their average diameter was found to be 119.82 nm. The chemical composition of TiO₂ NFs was confirmed by EDX analysis. The effects of Al₂O₃ NPs embedded TiO₂ nanofibers on the adsorption of dye and the charge transfer resistance were studied using UV-Vis spectroscopy and electrochemical AC-impedance studies. Dye sensitized solar cells fabricated using different weight percentages of Al₂O₃ NPs embedded TiO₂ NFs as photoanodes and Pt as counter electrode and 0.5M 1-butyl-3-methylimidazolium iodide, 0.5M LiI, 0.05M I₂, 0.5M 4-tertbutylpyridine in acetonitrile as the electrolyte. Among the three photoanodes tried, the cell fabricated using 3wt% of Al₂O₃ NPs embedded TiO₂ NFs as photoanode had an improved photocurrent efficiency (PCE) of 36.2% than the existing other similar systems in the literature. This might be due to an improvement in dye adsorption by the addition of a basic oxides (Al₂O₃) and also the formation of rutile phase (15.7%), thereby retarding the charge recombinations inside the DSSC and, in turn which increasing the V_{oc} and the J_{sc} of the cell.

Keywords: Titanium dioxide nanofibers, Alumina, Photoanode, Dye-sensitized solar cell, Electrospinning.

1. Introduction

Dye sensitised solar cells (DSSCs) are presently considered to be a promising candidate to replace the traditional p-n junction solar cells, which harvest the clean and inexhaustible energy of the sun and convert it into electricity. Involving low cost for fabrication and better solar conversion efficiency are the key factors for the attraction of researchers in this 3rd generation solar cell [1-3]. The most crucial part of a DSSC is the wide band gap semiconductor metal oxides which perform two important roles as being carrier for dye molecules and a transporter for the injected electrons. It has been found that the performance of DSSC depends mostly on photoanode material, since it influences both photocurrent and photovoltage of the solar cell. Among the various reported photoanode materials (TiO₂, ZnO, SnO₂, etc.), TiO₂ is found to exhibit high power conversion efficiency owing to its unique optoelectronic properties [4-7]. There are two ways to optimise DSSC photoanodes which will give an optimal light to electricity conversion.

First one is to enhance the charge transport and the other is minimizing charge recombination, which can be achieved by changing the morphology, porosity and crystallinity of the photoanodes. One dimensional (1D) nanostructured materials such as nanofibers, nanotubes, nanobelts, nanowires and nanorods showed better electron transport properties compared to nanoparticles based DSSCs [8,9]. In the case of one dimensional material, electron transport is faster because of the presence of lower grain boundaries, high connectivity and high surface area as seen in nanofibers. The nanofibers provide direct electric pathways to ensure rapid collection of charge carriers generated in the device.

Second one is to maximize the light harvesting capability of the device in that photoanode. This is done by using high surface area and high porosity, so as to adsorb maximum amount of dye. The nanofibers allow better filling of electrolyte in their pores

which improve the contact with the semiconductor and also help in regeneration of oxidized dyes, leading to high energy conversion efficiency [10, 11].

Surface modification of TiO_2 can be done by thin insulating oxides such as Y_2O_3 , MgO , Nb_2O_5 , ZnO and Al_2O_3 or using high band gap semiconductors to increase dye adsorption and thus to improve the photocurrent efficiency [12-16]. This difference is ascribed to the more basic nature of insulating oxides as compared to TiO_2 , favouring the dye attachment through its carboxylic acid groups. The voltage and fill factor of the cell are strongly enhanced due to the suppression of electron back transfer from TiO_2 to the redox electrolyte in the presence of the insulating oxide.

In the present investigation, we prepared for the first time, Al_2O_3 NPs embedded TiO_2 NFs by electrospinning technique and studied the influence of different wt% of Al_2O_3 NPs embedded TiO_2 nanofibers on the photovoltaic performances of DSSC.

2. Experimental Details

2.1 Preparation of Al_2O_3 NPs embedded TiO_2 NFs

Different weight percentages (1,3 and 5 wt%) of Al_2O_3 NPs embedded TiO_2 NFs were prepared by electrospinning technique (Fig. 1) using a precursor solution containing 0.01 M titanium (IV) isopropoxide (TiP, Aldrich) and 0.04 M acetic acid, different wt% of Al_2O_3 NPs, and 5 wt % polyvinylpyrrolidone (PVP: $M_w = 1300000$, Sigma Aldrich) in ethanol. After stirring for 6 h, the solution was loaded into a syringe equipped with a 27G stainless steel needle. The spinning rate (0.5 mL/min) was controlled using a syringe pump. The electric field of 15 kV was applied between a metal orifice and an electrically grounded flat collector. The collector was placed at 12 cm below the tip of the needle. The humidity level inside the electrospinning chamber was maintained below 35% at $\sim 25^\circ\text{C}$. The electrospun nanofibrous mats were removed from the collector and calcinated in a muffle furnace (Technico, India) at an increasing temperature rate of $5^\circ\text{C}/\text{min}$ from 30°C to 500°C to get different wt% of Al_2O_3 NPs embedded TiO_2 NFs.

Fig. 1

2.2 Characterization

The structural properties of different weight percentages of Al₂O₃ NPs embedded TiO₂ NFs were characterized by X-Ray diffraction studies (Rigaku, Ultima IV) over a range of 2θ angles from 20 to 80°. The scanning electron microscopy (Hitachi, Model: S-4200) coupled with EDX (Energy dispersive X-ray spectrometer) was employed to study surface morphology and the composition of different wt% of Al₂O₃ NPs embedded TiO₂ NFs. The morphologies of Al₂O₃ NPs embedded TiO₂ NFs were also probed using a transmission electron microscope (FEG-TEM, JSM-7600F). The absorption spectra were recorded by UV-Vis spectrophotometer (Perkin Elmer, Model: L- 650) to study the influence of different wt% of Al₂O₃ NPs embedded TiO₂ NFs on adsorption of the dye.

2.3 Fabrication of DSSC

FTO glass plates were cleaned with the help of detergent solution for 10 min, followed by cleansing in de-ionised water, acetone, and ethanol for 5 min each using an ultrasonic bath, and then they were dried in hot air. The pure TiO₂ NFs and Al₂O₃ NPs embedded TiO₂ NFs paste was prepared by the following method: as prepared Pure TiO₂ NFs/ Al₂O₃-TiO₂ NFs with PVP was stirred vigorously for 15 minutes followed by addition of 2mL ethanol and 0.3mL acetylacetone to avoid aggregation. Subsequently, 0.2 mL acetic acid was added. Finally 4-octylphenol polyethoxylate (Triton X-100) was added to act as a dispensing agent followed by 1 mL ethanol, PVP was used to increase the viscosity and adhesion property of paste and can easily decompose at 450°C during sintering [17]. The paste were coated with a thickness of 10-12 μm on FTO glass plates by the doctor blade technique and sintered at 450°C for 30 min. The active area of the cell was found to be 0.2 cm². After cooling to 80°C, the TiO₂ electrodes were immersed into the purified 0.3mM N719 dye solution [Di-tetrabutyl ammonium cis-bis (isothiocyanato) bis (2, 2'-bipyridyl - 4,

4'-dicarboxylato) ruthenium (II)] for 12 h at 30°C [18]. After completion of the dye adsorption, the films were rinsed with pure ethanol to remove the excess dye. In the counter electrode, a hole was drilled to pass the electrolyte later and subsequently cleaned in an ultrasonic bath with acetone and ethanol for 5 min. Then, a Pt paste was applied using the doctor blade technique, followed by sintering in a muffle furnace at 450°C for 30 min. A 60 μm surlyn spacer (SX 1170-60 from Solaronix) was sandwiched between the photoelectrode and the standard platinum coated FTO counter electrode. The space of each cell was filled with 0.5M LiI, 0.05M I₂, 0.5M 4-tertbutylpyridine in acetonitrile as the electrolyte by vacuum backfilling through the hole in the counter electrode. Finally, the hole was sealed with a hot-melt sheet and covered with a thin glass (0.1 mm).

2.4 Cell Studies

The Photovoltaic performances were measured using a computer controlled digital source meter. A Xe lamp with AM 1.5 filter (Oriel) was used to illuminate the DSSC at 100 mW cm⁻². Electrochemical AC-impedance measurements were carried out at room temperature in the frequency range of 1mHz to 100 kHz with the AC amplitude of 10mV to determine charge transfer resistance between the conducting oxide (FTO) and Al₂O₃ NPs embedded TiO₂ NFs and the interface between Al₂O₃ NPs embedded TiO₂ NFs | dye | electrolyte. The illumination condition for the impedance measurements was the same as that of J-V measurements.

3. Results and Discussion

3.1 X-Ray Diffraction studies

Fig. 2(a-d) represents the X-ray diffraction (XRD) patterns of pure TiO₂ NFs and Al₂O₃ NPs embedded TiO₂ NFs. Fig. 2 (a) shows that the TiO₂ NFs calcinations at 500°C has a single anatase phase. The diffraction peaks representing the crystal planes (101), (004), (200), (105), (116) and (215) corresponding to anatase phase matches with JCPDS data (Card No's 89-4920 and 89-4921) confirming the anatase phase. A small rutile phase along with anatase phase has synergistic effect in the efficient electron transport from rutile to anatase

than a single anatase phase [19-21]. An increase in wt% of Al₂O₃ NPs embedded in TiO₂ NFs, increased the percentage of rutile phase in TiO₂ NFs is shown in Fig. 2 (b-d). But, there was no peaks correspond to Al₂O₃ NPs were seen. The percentage of anatase/rutile was calculated from the X-ray diffractogram using the Spurr equation;

$$F_R = \frac{1}{1 + 0.8 [I_A(101) / I_R(110)]} \times 100$$

Where, I_A is the intensity of (101) peak and I_R is the intensity of (110) peak. The effect of different wt% of Al₂O₃ NPs embedded TiO₂ NFs on the formation of anatase and rutile phases is presented in Table 1. The formation of rutile phase is because of geometrical effects and hence the overall number of potential surface nucleation sites per unit volume will increase with a decrease in particle size. As the number of potential sites per unit volume increased, it would logically increase the number of surface nuclei and hence the rate of phase transformation also increased.

Fig. 2

Table 1

3.2 EDX analysis

X-ray diffraction study of Al₂O₃ NPs embedded TiO₂ NFs reveals no peaks for crystalline Al₂O₃ due to its very small wt% present in the samples. Table 2 presents EDX (Energy dispersive X-Ray Spectrometer) characterisation results. The amount of Al₂O₃ NPs embedded TiO₂ NFs and their corresponding EDX spectra are shown in Fig. 3 (a-d).

Fig. 3

Table 2

3.3 SEM analysis

Fig. 4 (a-b) show low resolution SEM images of as spun TiO₂ NFs and calcinated TiO₂ NFs. It was seen that the diameter of the nanofibers after calcination at 500°C showed an overall reduction of ~ 64.7 % in their average diameter with respect to as spun nanofibers, which was calculated as ~ 235 nm and ~ 83 nm for as spun and calcinated TiO₂ NFs,

respectively. It was also seen that the continuous nature of TiO₂ NFs after calcination remain unchanged without any loss in their continuity and some breakage were seen in the nanofibers. Fig.5 (a-d) shows SEM images of pure TiO₂ NFs and different wt% of Al₂O₃ NPs embedded TiO₂ NFs which were taken to further investigate for any change in the morphology of TiO₂ NFs. It was seen that no change in the morphologies occurred with the addition of Al₂O₃ NPs in TiO₂ NFs and the diameter of TiO₂ NFs also remain unchanged. The presence of Al₂O₃ NPs on TiO₂ NFs was not seen because of the low contrast. Hence, a further analysis was carried out using high resolution transmission electron microscopy (HRTEM). Fig. 6 (a) shows a representative TEM image of 3wt% of Al₂O₃ NPs embedded TiO₂ NFs. It can be seen that the 3wt% of Al₂O₃ NPs embedded over TiO₂ NFs as depicted by black dots. The TEM image of the interface between TiO₂ and Al₂O₃ NPs is displayed in Fig. 6 (b). The presence of the anatase TiO₂, Rutile TiO₂ phase, and Al₂O₃ NPs, can be seen clearly in Fig 6 (c). In Fig. 6 (d), the selected-area electron-diffraction (SAED) pattern confirms that the TiO₂ Nanofibers are composed of polycrystalline phase; i.e., the Debye–Scherrer concentric rings of (101), (004), (200), (105), (204), (220), and (215) planes. The SAED pattern has good agreement with the XRD results. Similarly, 1 and 5 wt% of Al₂O₃ NPs embedded TiO₂ NFs show the same microstructures with no appreciable differences.

Fig. 4

Fig. 5

Fig. 6

3.4 UV-Vis Spectral studies

The influence of different weight percentage of Al₂O₃ NPs embedded TiO₂ NFs on dye adsorption was carried out. TiO₂ NF paste was prepared using the following method; TiO₂ NFs with PVP were stirred in presence of ethanol and acetylacetone for 15 minutes, and acetic acid was added, subsequently. Finally, Triton X-100 was added as dispensing agent, followed by ethanol, then solution was concentrated by heating to obtain a viscous paste. These pastes were applied onto glass substrates by doctor blade technique using adhesive tape as a frame and spacer. For each Al₂O₃ NPs embedded TiO₂ films, two identical

photoanodes were fabricating and kept in air for 1 hr and then placed inside muffle furnace (Technico India) at 450°C for 30 minutes. After sintering, the glass substrates with different wt% of Al₂O₃ NPs embedded TiO₂ NFs based film, were placed in a dye bath containing 0.3mM cis- bis (isothiocyanato) bis -(2,2'bypyridyl-4,4' dicarboxylato) ruthenium(II) bistetrabutylammonium (N719) dye in ethanol for 24hr, keeping the sensitisation time same for all films so that we could avoid difference on the basis of time of sensitisation. The excess dye was removed by rinsing the surface of each glass substrates with ethanol. UV-Vis spectral studies were done in solid mode for the dye adsorbed on different wt% of Al₂O₃ NPs embedded TiO₂ NFs (Fig. 7). The increase in light absorbance by Al₂O₃ NPs was explained on the basis of increase in dye adsorption. The amount of dye adsorbed on the TiO₂ NFs significantly increased with the addition of Al₂O₃ NPs from 0 to 3wt%. The adsorption enhancement was related to an increase in Al₂O₃ NPs in TiO₂ NFs, which made the surface of TiO₂ NFs became more basic in nature in view of high isoelectric point of Al₂O₃ nanoparticles (~9.2). This helped to form strong chemisorption bonds with dye molecules via carboxylic ends of N719 dye [22]. This improved the solar cell performances [21-24]. But, in the addition of 5 wt% of Al₂O₃ NPs, the adsorption of dye on TiO₂ NFs decreased. This might be due to increase in amorphous nature on the surface of TiO₂ NFs, which reduced the overall surface area by blocking the porosity on the surface of the nanofibers, thereby reducing the dye adsorption [19,25]. To know about the effect on the absorption band gap with increase in wt% of Al₂O₃ NPs embedded in TiO₂ NFs, we measured the absorption band gap from the UV-Vis spectra using Origin Pro -9 and their values are given in Table. 1. It can be observed that there was a reduction in band gap from 3.20 eV to 3.00 eV by increasing the wt% of Al₂O₃ NPs from 1 to 5 wt% in TiO₂ NFs. The reduction in band gap is due to the addition of less valence cation (Al³⁺) than that of TiO₂ (Ti⁴⁺), which increased the concentration of oxygen vacancies, so that the charge balance was obtained. This was able to introduced a defect in the system that reduced the overall grain size which lead to contraction in the system, thereby reducing the bandgap.

Fig. 7

3.5 Electrochemical impedance studies

The electrochemical impedance study was carried to study the effect of different wt% of Al₂O₃ NPs embedded TiO₂ NFs on charge transfer resistance. Nyquist plot consisted of two semicircles (Fig. 8), corresponding to the charge transport resistance at counter electrode/electrolyte (R_{ct1}) at higher frequencies (kilohertz range) and at electrical contacts

between FTO/TiO₂ NFs or among TiO₂ NFs. The larger semicircle at lower frequencies corresponded to charge transfer resistance at TiO₂ NFs/dye/electrolyte interface (R_{ct2}) and the Warburg diffusion process of I/I₃⁻ redox couple in electrolyte (Z_w) at open circuit voltage under dark condition [26-28]. Though R_{ct2} virtually overlapped Z_w , the identical semicircles at higher frequency suggested that Al₂O₃ NPs embedded in TiO₂ NFs did not affect the charge transfer at counter electrode/electrolyte interface. R_{ct2} value decreased with the increase in Al₂O₃ NPs embedded in TiO₂ NFs upto 3wt% and then increased with further increase in Al₂O₃ NPs embedded in TiO₂ NFs. The variation in R_{ct2} value were in general consistent with the J_{sc} value of respective cell, i.e when the R_{ct2} value decreased, the J_{sc} value increased and vice versa. Increase in the Al₂O₃ NPs embedded in TiO₂ NFs from 3wt% to at 5wt%, led to increase in V_{oc} on expense of J_{sc} value. This is due to the reduction in dye adsorption and less electrolyte uptake, which led to decrease in overall device power conversion efficiency (PCE).

Fig. 8

Table 3

3.6 Photovoltaic measurements

Fig. 9 represents the current density- voltage (J - V) characteristics of DSSCs fabricated with various wt % Al₂O₃ NPs embedded TiO₂ NFs as photoanode. The DSSC fabricated using 3 wt % Al₂O₃ NPs embedded TiO₂ NFs as photoanode exhibited an improved power conversion efficiency of 36.2% with respect to DSSC fabricated using pure TiO₂ NFs. The obtained results were compared with the results reported for Al₂O₃ coated TiO₂ nanoparticles based DSSCs (Table 4). The Al₂O₃ NPs embedded TiO₂ NFs based DSSC exhibited higher percentage in PCE than the existing similar other systems reported in the literature [23, 29, 30]. The higher efficiency of the cell is due to reduction in the back carrier recombination by the addition of Al₂O₃ NPs, which have higher conduction band edge and higher band gap (7eV) than pure TiO₂ NFs (3.2 eV) allowing only a minor carrier flow to oxidise dye molecules or in other words to oxidise redox couple leading to an increase in conduction

band electrons as reflected by increase in J_{sc} . In the case of 5wt% of Al_2O_3 NPs embedded TiO_2 NFs, excess of Al_2O_3 decreased the dye adsorption and electrolyte uptake and increased the % of rutile phase, there by decreased the PCE. Table 5 summarizes the photovoltaic parameters of DSSCs based on different wt% of Al_2O_3 NPs embedded TiO_2 NFs.

Table 4

Fig. 9

Table 5

4. Conclusions

DSSC fabricated using 3 wt% of Al_2O_3 NPs embedded TiO_2 NFs exhibited an overall percentage of improvement in PCE of 36.2% compared to standard DSSC made from pure TiO_2 NFs as photoanode. This improvement also contributed to the presence of optimum rutile phase (15.7%) which helped in the synergetic effect to improve the electron transport easily from rutile to anatase phase. Both the above factors contributed to improve the dye adsorption and in turn the photovoltaic performance of the cell increasing both the V_{oc} and J_{sc} upto 3wt% of Al_2O_3 NPs embedded in TiO_2 NFs. But in 5 wt% of Al_2O_3 NPs embedded in TiO_2 NFs, the dye adsorption lowered and offered high resistance to flow of electrons across TiO_2 NFs| Al_2O_3 |dye| electrolyte interface. An increase in J_{sc} of the cell was in agreement with the decrease in resistance upto 3wt% of Al_2O_3 NPs embedded in TiO_2 NFs. With further increase of Al_2O_3 NPs embedded in TiO_2 NFs, the resistance to flow of electrons across TiO_2 NFs/dye/electrolyte (R_{ct2}) increased, because of increase in the tunnelling length by large number of Al_2O_3 NPs on the surface of TiO_2 that hindered the electron injection, leading to decrease in J_{sc} also the efficiency of the cell. Thus 3wt% of Al_2O_3 NPs embedded TiO_2 NFs with 15.7% rutile phase could be used as an effective photoanode for DSSC to improve the efficiency of the cell.

Acknowledgements

The authors gratefully acknowledge the CSIR (Ref. No.01(2359)/10/EMR-II , New Delhi for the financial support.

References

- [1] B. O Regan and M. Gratzel, *Nature*, 1991, **353**, 737-740.
- [2] M. Gratzel, *Nature*, 2001, **414**, 338-344.
- [3] Hagfeldt and M. Gratzel, *Acc. Chem. Res.*, 2000, **33**, 269-277.
- [4] Y. G. Guo, Y. S. Hu and W. Sigle, J. Maier, *Adv. Mater.*, 2007, **19**, 2087-2091.
- [5] S. A. Akbar, L. B. Younkman and P. K. Dutta, *ACS Symp. Ser.*, 1998, **690**, 161-167.
- [6] M. K. Nazeeruddin, F. De Angelis, S. Fantacci, A. Selloni, G. Viscardi, P. Liska, S. Ito, B. Takeru and M. G. Gratzel, *J. Am. Chem. Soc.*, 2005, **127**, 16835-16847.
- [7] A. Fujishima and K. Honda, *Nature*, 1972, **238**, 37-38.
- [8] A. C. Fisher, L. M. Peter, E. A. Ponomarev, A. B. Walker and K. G. U. Wijayantha, *J. Phys. Chem., B*, 2000, **104**, 949-958.
- [9] J. Bisquert and V. S. Vikhrenko, *J. Phys. Chem. B*, 2004, **108**, 2313-2322.
- [10] K. Onozuka, B. Ding, Y. Tsuge, T. Naka, M. Yamazaki, S. Sugi, S. Ohno, M. Yoshikawa and S. Shiratori, *Nanotechnology*, 2006, **17**, 1026-1031.
- [11] M. Y. Song, Y. R. Ahn, S. M. Jo, D. Y. Kim and J.-P. Ahn, *Appl. Phys. Lett.*, 2005, **87**, 113113-3.
- [12] E. Palomares, J.N. Clifford, S.A. Haque, T. Lutz and J.R. Durrant, *J. Am. Chem. Soc.*, 2003, **125**, 475-482.
- [13] A. Kay and M. Gratzel, *Chem. Mater.*, 2002, **14**, 2930-2935.
- [14] Zhong-Sheng Wang, Chun-Hui Huang, Yan-Yi Huang, Yuan-Jun Hou, Pu-Hui Xie, Bao-Wen Zhang and Hu-Min Cheng, *Chem. Mater.*, 2001, **13**, 678-682.
- [15] S. G. Chen, S. Chappel, Y. Diamant and A. Zaban, *Chem. Mater.*, 2001, **13**, 4629-4634.
- [16] H. Alarcon, G. Boschloo, P. Mendoza, J. L. Solis and A. Hagfeldt, *J. Phys. Chem. B*, 2005, **109**, 18483-18490.

- [17] S.N. Karthick, K.V. Hemalatha, C. Justin Raj, A. Subramania, Hee-Je Kim, *Thin Solid Films*, 2012, **520**, 7018-7021.
- [18] A. Subramania, E. Vijayakumar, N. Sivasankar, A. R. Sathiya Priya and Kang-Jin Kim, *Ionics*, 2013, **19**, 1649-1653.
- [19] Tae Kwan Yun, Sung Soo Park, Duckhyun Kim, Jae-Hyun Shim, Jae Young Bae, Seong Huhc and Yong Sun Won, *Dalton Trans.* 2012, **41**, 1284-1288.
- [20] Jianning Ding, Yan Li, Hongwei Hu, Li Bai, Shuai Zhang and Ningyi Yuan, *Nanoscale Res Lett.*, 2013, **8**, 5-9.
- [21] G.H. Li, C.P. Richter, G.W. Brudvig and V.S. Batista, *Dalton Trans.*, 2009, **45**, 10078-10085.
- [22] X.T. Zhang, I. Sutanto, T. Taguchi, K. Tokuhira, Q.B. Meng, T.N. Rao, A. Fujishima, H. Watanabe, T. Nakamori, and M. Urugami, *Solar Energy Mater. & Solar Cells*, 2003, **80**, 315-326.
- [23] V. Ganapathy, B. Karunakaran and Shi-Woo Rhee, *J. Power Sources*, 2005, **195**, 5138-5143.
- [24] C.P. Lee, P.Y. Chen, R. Vittal and K.C. Ho, *Phys, Chem. Chem. Phys.*, 2010, **12**, 9249-9255.
- [25] E. Barajas-Ledesma, M.L. Garcia-Benjume, I. Espitia-Cabrera, M. Ortiz-Gutierrez, F.J. Espinoza-Beltran, J. Mostaghine and M.E. Contreras-Garcia, *Mater. Sci. Engg. B*, 2010, **174**, 71-73.
- [26] L. Han, N. Koide, Y. Chiba and T. Mitate, *Appl. Phys. Lett.*, 2004, **84**, 2433-2435.
- [27] Z. Zhang, S. M. Zakeeruddin, B. O Regan, R. Humphry-Baker and M. Gratzel, *J. Phys. Chem. B.*, 2005, **109**, 21818-24.
- [28] R. Kern, R. Sastrawan, J. Ferber, R. Stangl and J. Luther, *Electrochim. Acta.*, 2002, **47**, 4213-4225.

- [29] Emilio Palomares, John N. Clifford, Saif A. Haque, Thierry Lutz and R James, *Chem. Commun.*, 2002, **14**, 1464-1465.
- [30] Xin-tong Zhanga, Irwan Sutantoa, Taketo Taguchia, Kenichi Tokuhiroa, Qing-bo Menga, Tata N. Raoa, Akira Fujishimaa, Hiroko Watanabeb, Toshie Nakamorib and Masayuki Uragami, *Sol. Energy Mater. Sol. Cells*, 2003, **80**, 315-326.

Figure Captions

Fig. 1 Schematic illustration for electrospinning of Al₂O₃ NPs embedded TiO₂ nanofibers.

Fig. 2 XRD patterns of TiO₂ Nanofibers and Al₂O₃ NPs embedded TiO₂ NFs.

Fig. 3 EDX spectra of a) Pure TiO₂ NFs b) 1wt% Al₂O₃ NPs embedded TiO₂ NFs c) 3wt% Al₂O₃ NPs embedded TiO₂ NFs d) 5wt% Al₂O₃ NPs embedded TiO₂ NFs.

Fig. 4 SEM images of (a) as-spun TiO₂ NFs and (b) Calcinated TiO₂ NFs.

Fig. 5 SEM images of different wt% of Al₂O₃ NPs embedded TiO₂ NFs (a) 0 wt%. (b) 1 wt%. (c) 3 wt% and (d) 5 wt% after calcination at 500°C.

Fig. 6 TEM images of the 3 wt% of Al₂O₃ NPs embedded TiO₂ NFs: (a) Bright field image; (b &c) High resolution images at different magnifications, and (d) SAED pattern.

Fig. 7 UV-Vis spectra of different wt% of Al₂O₃ NPs embedded TiO₂ NFs on adsorption of N719 dye.

Fig. 8 Nyquist Plots of DSSCs fabricated with different wt% of Al₂O₃ NPs embedded TiO₂ NFs.

Fig. 9 Photocurrent density-voltage characteristics of DSSCs fabricated with different wt% of Al₂O₃ NPs embedded TiO₂ NFs.

Tables

Table 1 Effect of different wt% of Al₂O₃ NPs embedded TiO₂ NFs on the formation of anatase and rutile phases and their absorption band gap.

Weight % of Al ₂ O ₃ NPs in TiO ₂ NF's	% of Anatase Phase	% of Rutile Phase	Absorption band gap (eV)
0	100.0	0	3.20
1	91.6	8.4	3.14
3	84.6	15.7	3.06
5	82.8	17.2	3.00

Table 2 EDX elemental map showing distribution of Ti, Al, and O, atoms in different wt% of Al₂O₃ NPs embedded TiO₂ NFs.

Composition of NFs	Titanium wt (%)	Aluminum wt (%)	Oxygen wt (%)
Pure TiO ₂ NFs	23.01	0.00	76.99
1wt% Al ₂ O ₃ in TiO ₂ NFs	64.76	0.59	34.65
3wt% Al ₂ O ₃ in TiO ₂ NFs	42.83	0.92	56.25
5wt% Al ₂ O ₃ in TiO ₂ NFs	39.98	0.97	59.05

Table 3 EIS parameters of R_s, R_{ct1} and R_{ct2} values for DSSCs fabricated using pure TiO₂ NFs and Al₂O₃ NPs embedded TiO₂ NFs.

Photoanode	R _s	R _{ct1} (Ωcm ⁻²)	R _{ct2} (Ωcm ⁻²)
Pure TiO ₂ NFs.	15.06	6.89	23.84
1wt% Al ₂ O ₃ - TiO ₂ NFs	14.85	7.20	21.54
3wt% Al ₂ O ₃ - TiO ₂ NFs	14.70	6.17	18.42
5wt% Al ₂ O ₃ - TiO ₂ NFs	14.00	7.10	20.50

Table 4 Photovoltaic parameters of DSSCs fabricated with different wt% of Al₂O₃ NPs embedded TiO₂ nanofibers.

Photoanode	J _{sc} (mA cm ⁻²)	V _{oc} (V)	FF	η (%)
Pure TiO ₂ NFs	10.3	0.64	73	4.81
1% Al ₂ O ₃ - TiO ₂ NFs	10.8	0.66	75	5.35
3% Al ₂ O ₃ - TiO ₂ NFs	11.7	0.70	80	6.55
5% Al ₂ O ₃ - TiO ₂ NFs	11.0	0.72	76	5.85

Table 5 Comparison of photovoltaic performances of DSSCs fabricated by using Al₂O₃ coated TiO₂ as photoanodes.

Photoanode	V _{oc} (mV)	J _{sc} (%)	FF (%)	Cell efficiency (%)	% of improvement in PCE (%)	Ref.
TiO ₂ /Al ₂ O ₃ core shell	705.6	19.0	63	8.4	35.5	[23]
Al ₂ O ₃ coated nanoporous TiO ₂ films	750	10.9	65	5.0	30.0	[29]

Al ₂ O ₃ coated nanoporous TiO ₂	470	9.5	52	2.6	33.5	[30]
Al ₂ O ₃ NPs embedded TiO ₂ NFs	750	11.7	80	6.55	36.2	Present work

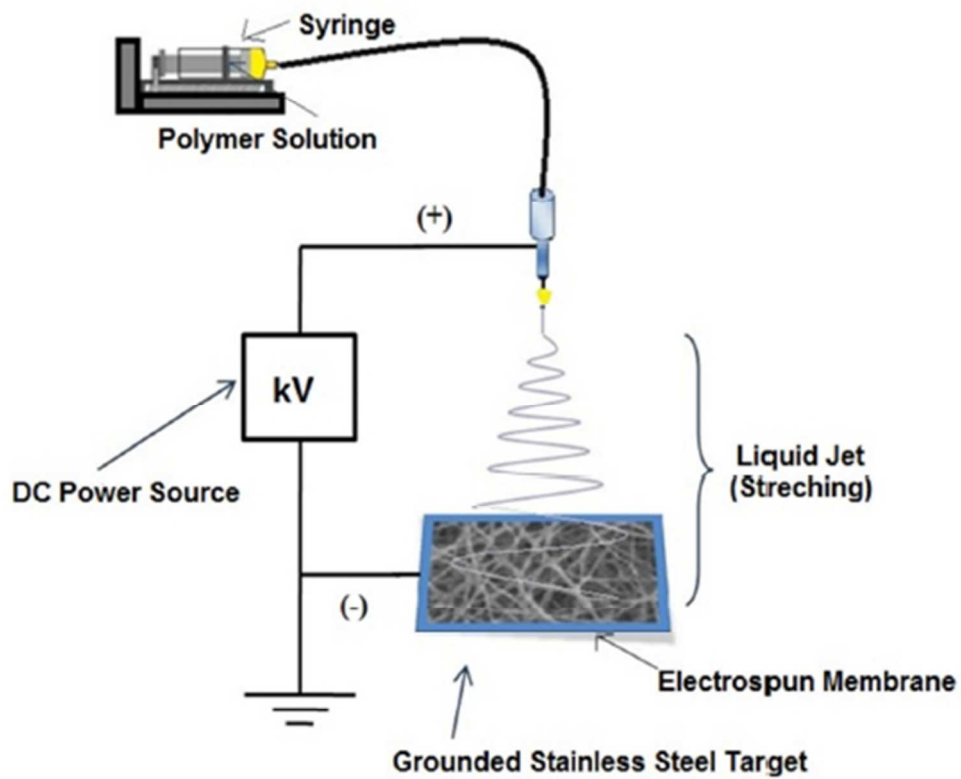


Fig. 1 Schematic illustration for electrospinning of Al_2O_3 NPs embedded TiO_2 nanofibers.
43x35mm (300 x 300 DPI)

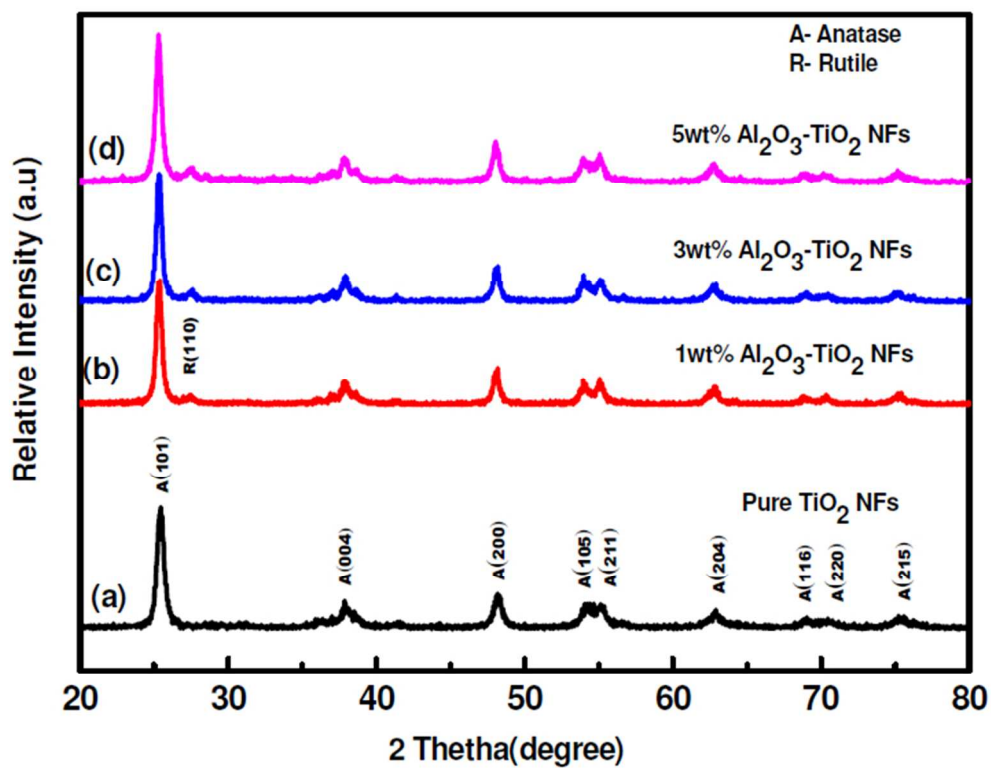


Fig. 2 XRD patterns of TiO₂ Nanofibers and Al₂O₃ NPs embedded TiO₂ NFs.
61x48mm (300 x 300 DPI)

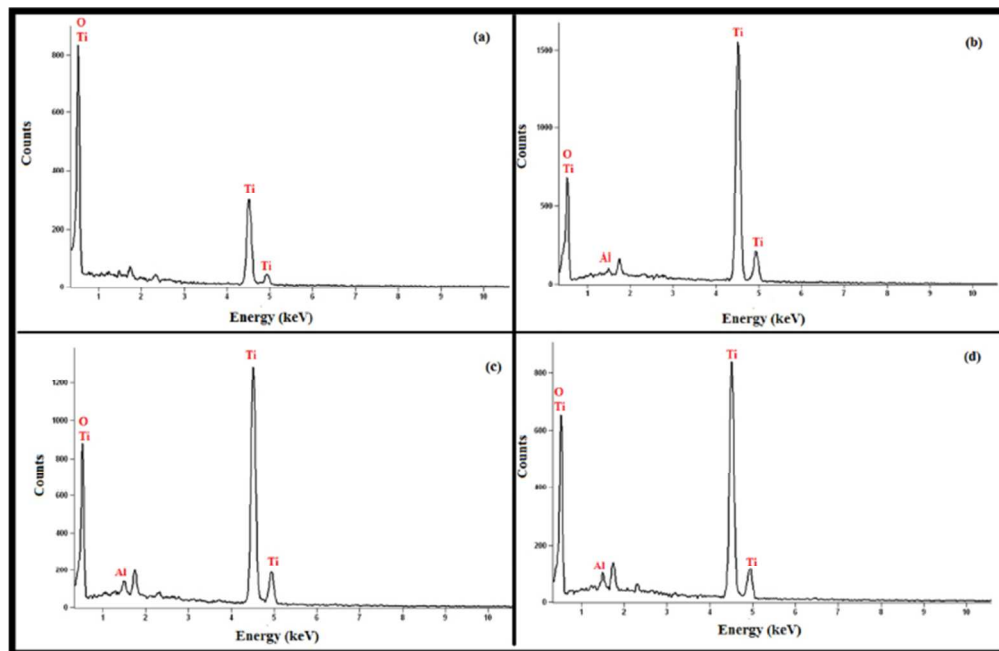


Fig. 3 EDX spectra of a) Pure TiO₂ NFs b) 1wt% Al₂O₃ NPs embedded TiO₂ NFs c) 3wt% Al₂O₃ NPs embedded TiO₂ NFs d) 5wt% Al₂O₃ NPs embedded TiO₂ NFs.
66x43mm (300 x 300 DPI)

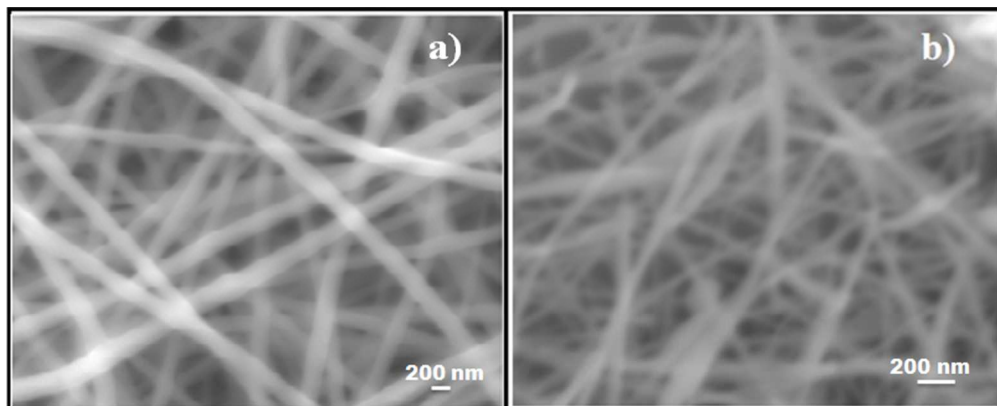


Fig. 4 SEM images of (a) as-spun TiO₂ NFs and (b) Calcinated TiO₂ NFs.

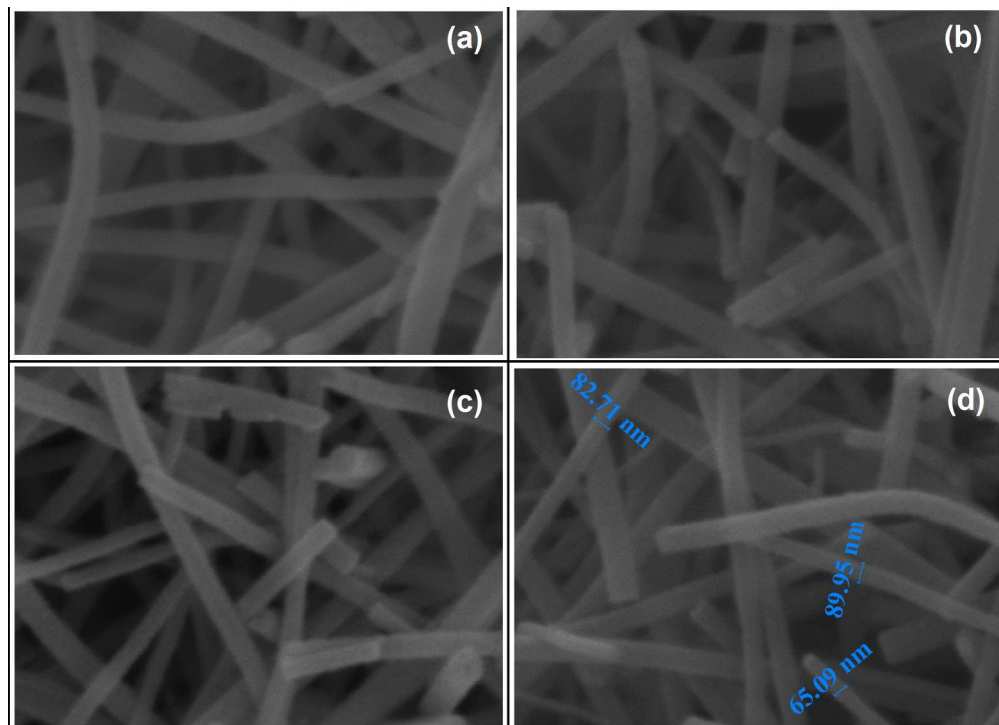


Fig. 5 SEM images of different wt% of Al₂O₃ NPs embedded TiO₂ NFs (a) 0 wt%. (b) 1 wt%. (c) 3 wt% and (d) 5 wt% after calcination at 500°C.
177x128mm (300 x 300 DPI)

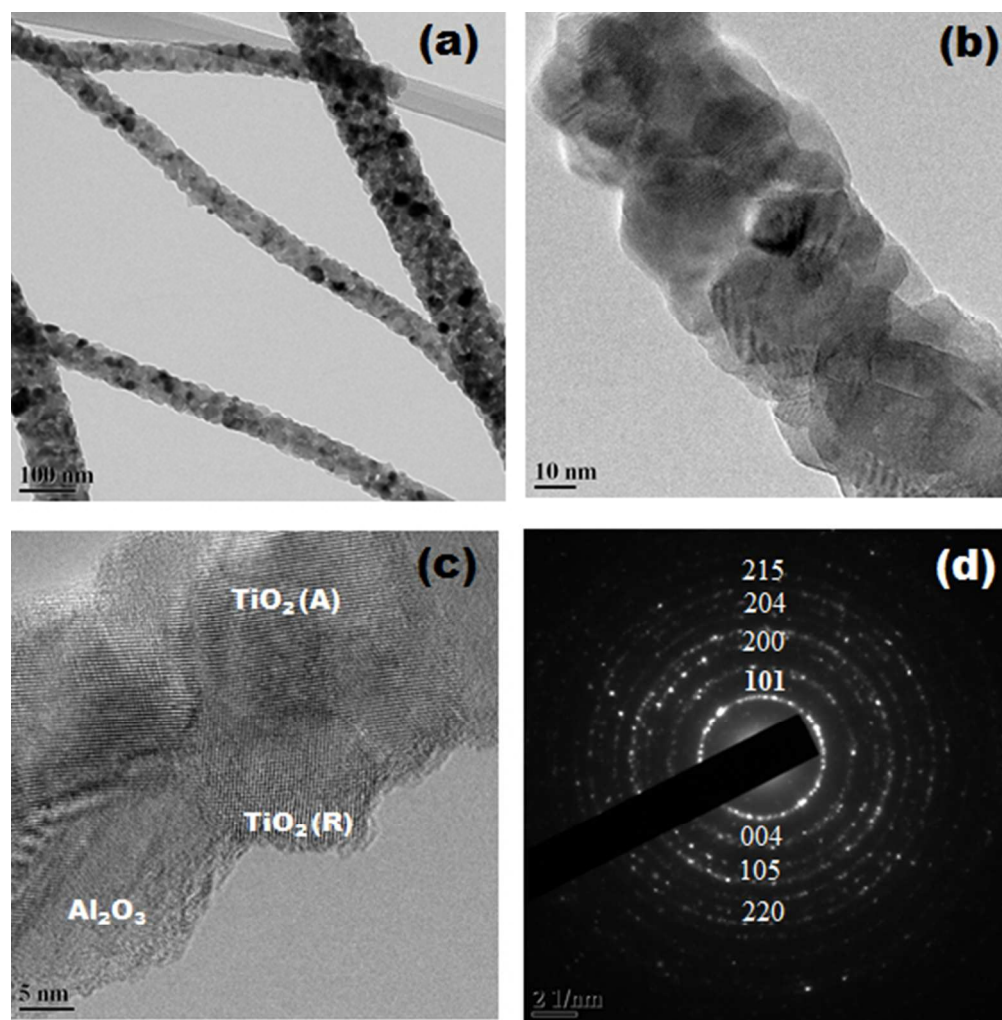


Fig. 6 TEM images of the 3 wt% of Al₂O₃ NPs embedded TiO₂ NFs: (a) Bright field image; (b &c) High resolution images at different magnifications, and (d) SAED pattern.
47x48mm (300 x 300 DPI)

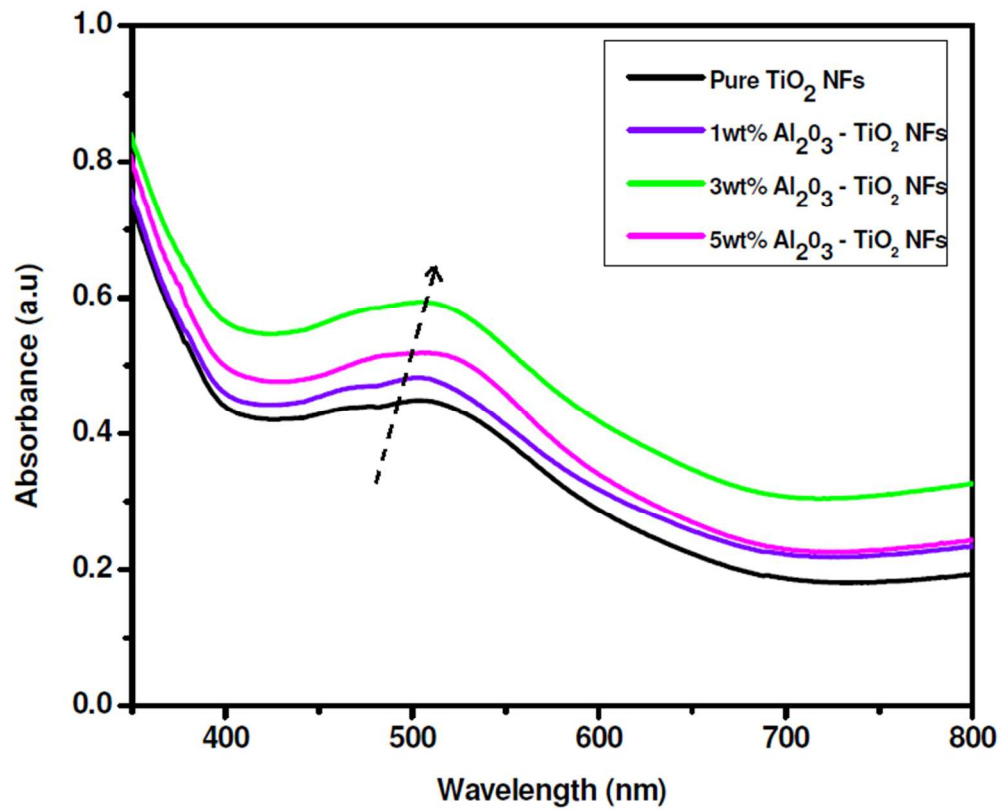


Fig. 7 UV-Vis spectra of different wt% of Al₂O₃ NPs embedded TiO₂ NFs on adsorption of N719 dye.
65x53mm (300 x 300 DPI)

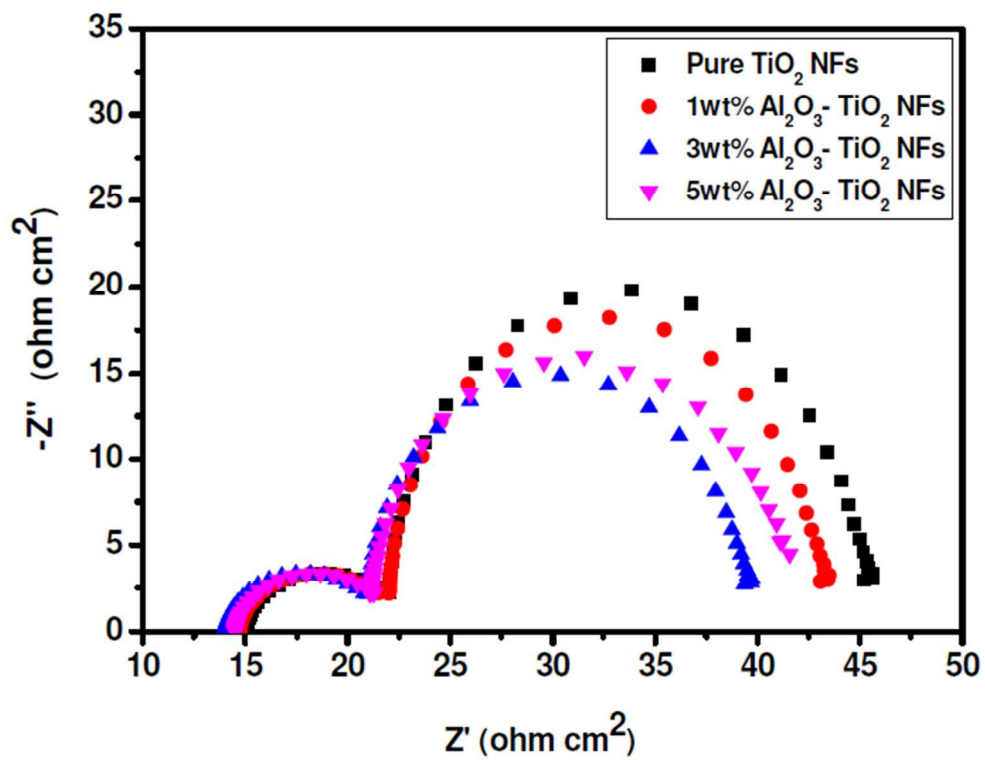


Fig. 8 Nyquist Plots of DSSCs fabricated with different wt% of Al_2O_3 NPs embedded TiO_2 NFs.
59x46mm (300 x 300 DPI)

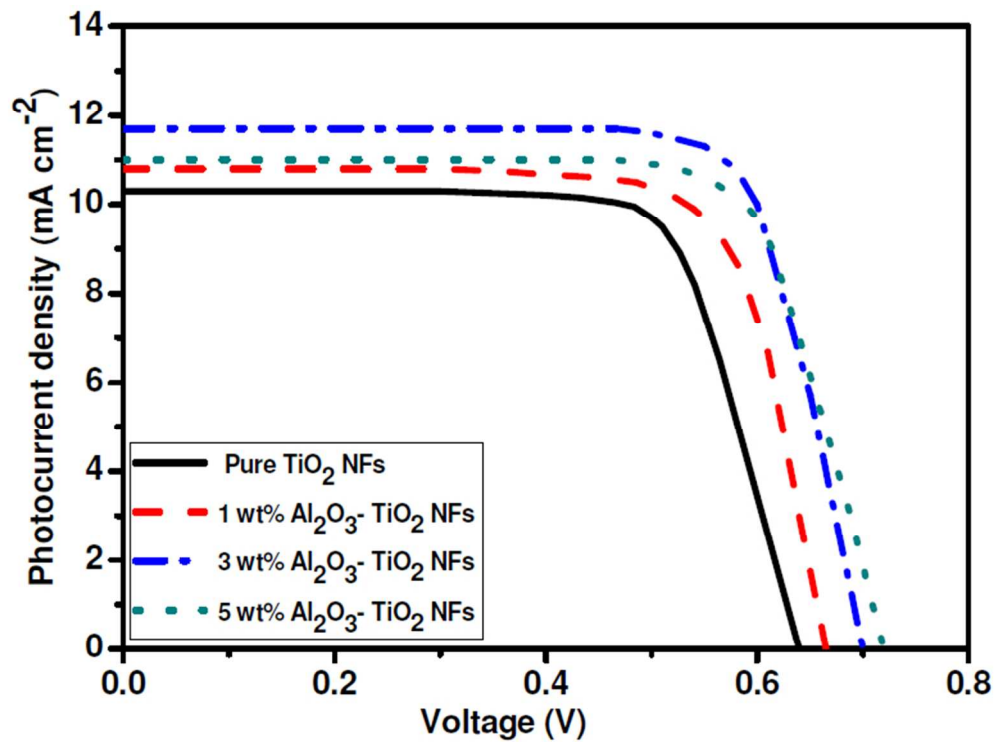
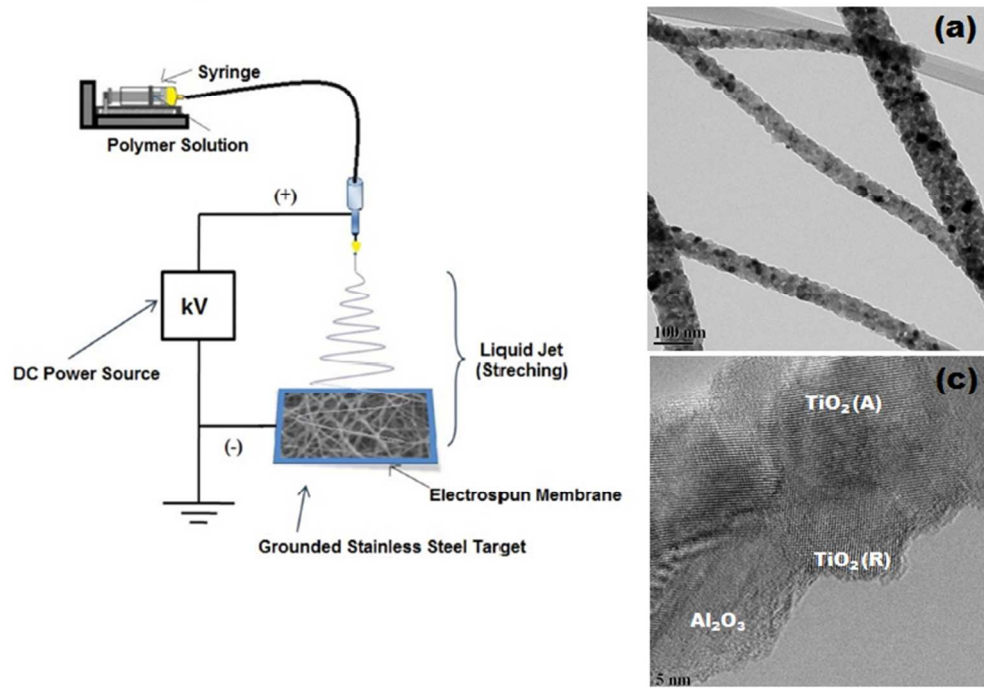


Fig. 9 Photocurrent density-voltage characteristics of DSSCs fabricated with different wt% of Al₂O₃ NPs embedded TiO₂ NFs.
66x49mm (300 x 300 DPI)



67x46mm (299 x 299 DPI)